Title

Ultrashort echo time T2 values decrease in tendons with application of static tensile loads

Authors

Jerban, Saeed
Nazaran, Amin
Cheng, Xin
et al.

Publication Date

2017

DOI

10.1016/j.jbiomech.2017.07.018

Journal of Biomechanics 61 (2017) 160–167

Contents lists available at ScienceDirect

Journal of Biomechanics

journal homepage: www.elsevier.com/locate/jbiomech
www.JBiomech.com

Ultrashort echo time T2* values decrease in tendons with application of static tensile loads

Saeed Jerban [a,*], Amin Nazaran [a], Xin Cheng [a,b], Michael Carl [c], Nikolaus Szeverenyi [a], Jiang Du [a], Eric Y. Chang [d,a]

[a] Department of Radiology, University of California, San Diego, CA, USA
[b] Department of Histology and Embryology, Jinan University, Guangzhou, China
[c] GE Healthcare, San Diego, CA, USA
[d] Radiology Service, VA San Diego Healthcare System, San Diego, CA, USA

ARTICLE INFO

Article history:
Accepted 16 July 2017

Keywords:
Tendon
Tensile loading
MRI
Ultrashort TE
T2*

ABSTRACT

In early stages of tendon disease, mechanical properties may become altered prior to changes in morphological anatomy. Ultrashort echo time (UTE) magnetic resonance imaging (MRI) can be used to directly detect signal from tissues with very short T2 values, including unique viscoelastic tissues such as tendons. The purpose of this study was to use UTE sequences to measure T2*, T1 and magnetization transfer ratio (MTR) variations of tendon samples under static tensile loads. Six human peroneal tendons were imaged before and under static loading using UTE sequences on a clinical 3 T MRI scanner. Tendons were divided into two static tensile loading groups: group A that underwent one-step loading (15 N) and group B that underwent two-step loading (15 and 30 N). The T2*, T1 and MTR variations were investigated in two selected section regions of interest (ROIs), including whole and core sections. Mean T2* values for the first step of loading (groups A and B) in both whole section and core section ROIs were significantly decreased by 13 ± 7% (P = 0.028) and 16 ± 5% (P = 0.017), respectively. For the second loading step (group B), there was a consistent, but non-significant reduction in T2* value by 9 ± 2% (P = 0.059) and 7 ± 5% (P = 0.121) for whole and core sections, respectively. Mean T1 did not show any consistent changes for either loading steps (P > 0.05). Mean MTR increased slightly, but not significantly for both loading steps (P > 0.05). Significant differences were found only in T2* values of tendons by static tensile load application. Therefore, T2* monitoring during loading is suggested for quantitative investigation of the tendons biomechanics.

1. Introduction

Tendons are unique viscoelastic connective tissues that are responsible for transferring the mechanical loads generated by muscles to the bones (Aparecida de Aro et al., 2012; Franchi et al., 2007b). Water, as the main viscous component (Wellen et al., 2005) of tissues, may comprise over 60% of the total tendon weight (Aparecida de Aro et al., 2012)). Of the dry weight of the tendon, 60–85% is composed of highly organized collagenous fibers, particularly collagen type I (Aparecida de Aro et al., 2012). Collagenous fibers count for the elastic component of tendons (Wellen et al., 2005). The mechanical properties and great strength of tendons can be partially explained by their highly organized and hierarchical structure, which consist of collagen fibrils, fibers, bundles of fibers and fascicles (Aparecida de Aro et al., 2012; Khan et al., 1999). Tendons demonstrate crimp or zigzag patterns in their microstructure that enable them to withstand, up to 3% strain without damage (Aparecida de Aro et al., 2012; Hansen et al., 2002; Khan et al., 1999).

Magnetic resonance (MR) imaging, as a non-invasive modality, is routinely used for the diagnosis of tendon disease (Pierre-Jerome et al., 2010). The detected signal intensity of a tissue in MR imaging depends on various factors including relaxation time of transverse magnetization (T2) (Chang et al., 2015b; Hendee and Morgan, 1984). Tendons possess a high percentage of organized collagenous matrix that results in very short T2 (Chang et al., 2015b). Therefore, tendon is represented as very low signal intensity when imaged with conventional clinical MR sequences, similar to background noise (Chang et al., 2015b; Du et al., 2010b; Juras et al., 2012). Specifically, the tendon transverse magnetization decays faster than the capability of conventional

* Corresponding author at: Department of Radiology, University of California, 9500 Gilman Dr, San Diego, CA 92093, USA.
E-mail address: sjerban@ucsd.edu (S. Jerban).

http://dx.doi.org/10.1016/j.jbiomech.2017.07.018
0021-9290/

MRI sequences to capture the signal. However, by using ultrashort echo time (UTE) imaging techniques, signal can be detected in tendons (Chang et al., 2015b; Du et al., 2010b; Jerban et al., 2017; Juras et al., 2013, 2012; Nazaran, 2016; Nazaran et al., 2017). In UTE-MRI, signal can be acquired at very short echo times (on the order of tens of microseconds), before complete decay of transverse magnetization (Chang et al., 2015b; Du et al., 2010b; Juras et al., 2012). In addition to improved visualization, UTE-MRI allows quantitative analysis of the MRI-based properties of tendons, such as apparent relaxation time of transverse magnetization (T2*), relaxation time of longitudinal magnetization (T1), and magnetization transfer (MT) measurements such as MT ratio (MTR) (Chang et al., 2015b,2014a, 2014b,Du et al., 2010a,2010b Juras et al., 2013, 2012; Koff et al., 2014; Syha et al., 2014). Such quantitative UTE biomarkers are hypothesized to reflect histologic changes such as degeneration, including collagen disorganization and increases in total water content (Juras et al., 2013, 2012; Khan et al., 1999; Nazaran et al., 2017; Syha et al., 2014).

Early stage diagnosis of tendon diseases is of great interest to the musculoskeletal research community. Different diseases are hypothesized to alter the mechanical performance of tissues earlier than changes in their anatomical morphology. Hence, researchers have attempted to monitor the changes in MR imaging biomarkers after tensile loading in tendon to assess the sensitivity to mechanical alterations (Han et al., 2000; Helmer et al., 2006, 2004; Koff et al., 2014; Mountain et al., 2011; Shao et al., 2016; Syha et al., 2014; Wellen et al., 2005, 2004), however, only a few of them have used UTE-MRI (Koff et al., 2014; Shao et al., 2016; Syha et al., 2014).

During tendon stretching, two main phenomena occur; first, the number of crimps decrease and the mean crimp angle flattens (Franchi et al., 2007a, 2007b; Legerlotz et al., 2014; Morgan et al., 2006; Mountain et al., 2011), and second, free water redistributes within (Helmer et al., 2004; Wellen et al., 2005, 2004) and outside the tissue (Han et al., 2000; Hannafin and Arnoczky, 1994). In addition, the diameter of larger collagen fibrils decreases and less interspace areas can be found in loaded tendons (Morgan et al., 2006). Therefore, MRI properties of tendons may be expected to change under mechanical loading, even though reported changes in the literature have been inconsistent and are not well understood.

Among the few reported UTE-MRI based studies of tendons under the mechanical loading, Syha et al. observed significant increase of UTE-MTR in vivo (i.e., off-resonance radiofrequency saturation ratio, ORS) for tendons, after short-term exercises (Syha et al., 2014). Chang et al. (2015a) also observed a significant increase in UTE-MTR in human tendon under static tensile loads (5–10 N). Koff et al. used UTE-MRI for imaging of cyclically loaded (100 cycles of 45 N) rabbit patellar tendon (Koff et al., 2014). The tendons presented significantly shorter T2* values after cyclic loading. In our previous study, (Chang et al., 2015c), UTE-MRI was used for assessing statically loaded human tendons by 10 N loads. No significant changes in UTE biomarkers were observed using single- and bi-component T2* analyses. The applied load in our previous study (Chang et al., 2015c), may have been too low to exert significant changes in the tendons, similar to the fact that (Helmer et al., 2004) did not observe changes in rabbit Achilles tendons when only 5 N tensile load was applied.

The main objective of this study was to determine whether the application of higher static tensile loads (>10 N) on human tendons alter T2*, T1, and MTR as measured using UTE sequences.

2. Material and methods

2.1. Sample preparation

Six peroneal tendon samples (longus and brevis) were harvested from the ankles of three donors (all female; 38-, 40- and 95-year-old). Tendon samples were cut into 6 cm length and then distributed into two groups. One sample from each donor (longus or brevis) was selected randomly for group A to undergo a one-step loading protocol (15 N). The three remaining samples were assigned to group B and underwent a two-step loading protocol (15 and 30 N). Tendon samples were subjected to two cycles of freezing and thawing. All samples were immersed in saline for 2 h at 4 °C and gently mounted into a plastic loading device fabricated in-house. During the mounting and installing process, the samples were kept hydrated using saline. The loading device chamber was filled with perfluoropolyether (Fomblin, Ausimont, Thorofare, NJ) to minimize dehydration and susceptibility artifact.

2.2. Mechanical loading

An MRI compatible loading device was fabricated using a plastic spring (LL075100U40G, Lee Spring, Brooklyn, NY). The spring was compressed by a manually driven screw, mounted on a notched standard 1 × 6-inch polyvinyl chloride (PVC) pipe (Fig. 1a). Two sides of the tendon specimens were clamped in "fixed" and "sliding" grippers placed on the notched pipe. The two ends of the tendon were fixed firmly in the grippers using two sets of 1/4-inch Nylon bolts and nuts (Fig. 1b). The applied tensile mechanical load was calculated based on the amount of spring deformation and its stiffness. The stiffness of springs was calculated by the manufacturer using a load tester machine (UT 11, Larson Systems Inc., Minneapolis, MN, USA) after four loading sessions from 0 to maximum compression (i.e., 2.5, 5.0, 7.5, 10.0, and 15 mm). This was aimed to reduce the initial plastic creep, to achieve an accurate stiffness value and, more importantly, to reduce stiffness changes along the loading experiment in MRI. Along the four loading sessions, the average calculated stiffness converged from 2.10 to 1.98 N/mm.

For the scans during the unloaded stage, the screw was driven gently until the beginning of spring deformation (1 N approx.) to make sure that the tendon samples were straight. For the scans at loading stage, the load was adjusted after 2 min approximately prior to scanning to compensate the limited relaxation of the tendon.

2.3. UTE-MRI sequences

The loading device and specimens were placed parallel to the B0 field and imaged in the axial plane on a clinical 3 T MRI scanner (Signa HDx, GE Healthcare Technologies, Milwaukee, WI) using a wrist coil (BC-10, Medspira, Minneapolis, MN). A quantitative imaging protocol was performed, consisting of I) dual-echo 3D-UTE-Cones sequences (TR = 24.3 ms, TEs = 0.032, 0.4, 0.8, 4.4, 8.8, 13 ms) for T2*measurements, II) variable TR 3D-UTE-Cones sequences (TE = 0.032 ms, TRs = 7.3, 15, 30, 50, 80 ms) for T1 measurements, and III) 3D-UTE-MT-Cones sequences (MT pulse power = 1500°, frequency offset = 2, 5, 10 kHz plus one acquisition without MT preparation) for MTR calculations. Total scan time was 8:36, 20:08, and 7:28 for dual-echo 3D-UTE, variable TR 3D-UTE, and 3D-UTE-MT sequences, respectively. Other imaging parameters include field of view (FOV) = 4 cm, acquisition matrix = 192 × 192, slice thickness = 3 mm, number of slices = 20, flip angle = 10° and receive bandwidth = 62.5 kHz.

2.4. Data analysis

For each dataset, two regions of interest (ROIs) were selected covering the whole and core regions of the tendons (Fig. 2). Single-component fitting models were utilized for T2* decay ($S(TE) \propto \exp(-TE/T2^{*}) + constant$) and T1 recovery ($S(TR) \propto 1 - \exp(-TR/T1) + constant$) analyses. The MTR for each off-resonance frequency was calculated by the following equation: $MTR = (S_0 - S_{SAT})/S_0$, where S_0 denotes the mean signal intensity acquired without a saturation pulse and S_{SAT} denotes the mean signal intensity acquired with the saturation pulse. All analyses were performed using an in-house developed code in MATLAB (Mathworks, Natick, MA, USA). The T2*, T1 and MTR values as well as their pixel maps in loaded tendon samples were compared with the same samples before loading.

2.5. Statistical analysis

All statistical analyses were performed using a statistical programming language (R, version 3.2.5, R Development Core Team, Vienna, Austria). The average values of T2*, T1 and MTR in unloaded and loaded tendons were compared using the two-tailed paired t-student test. P-values below 0.05 were considered significant.

3. Results

Fig. 2 shows the single component exponential decay fitting at the three loading conditions (non-loaded, 15, and 30 N, respectively) for two selected ROIs (whole section and the core section) of representative sample B-1. The fitting curves demonstrated very good agreements with the actual data for both of the ROIs. The calculated T2* values showed a decrease for both the whole and the core sections after application of the first loading step (15 N),

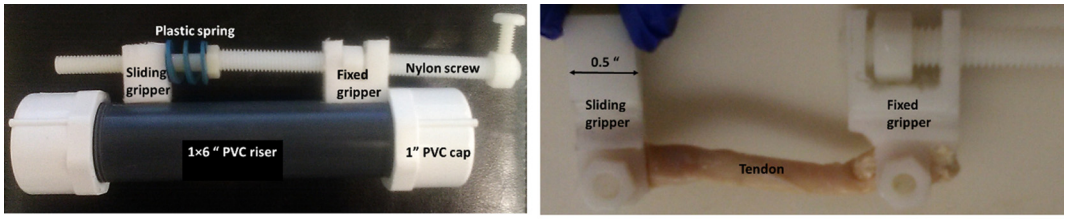

Fig. 1. (a) MRI compatible, plastic, loading device used for applying static extension loads on peroneal tendons soaked in fomblin. (b) Mounted tendon on the fixed and sliding grippers, using plastic bolts.

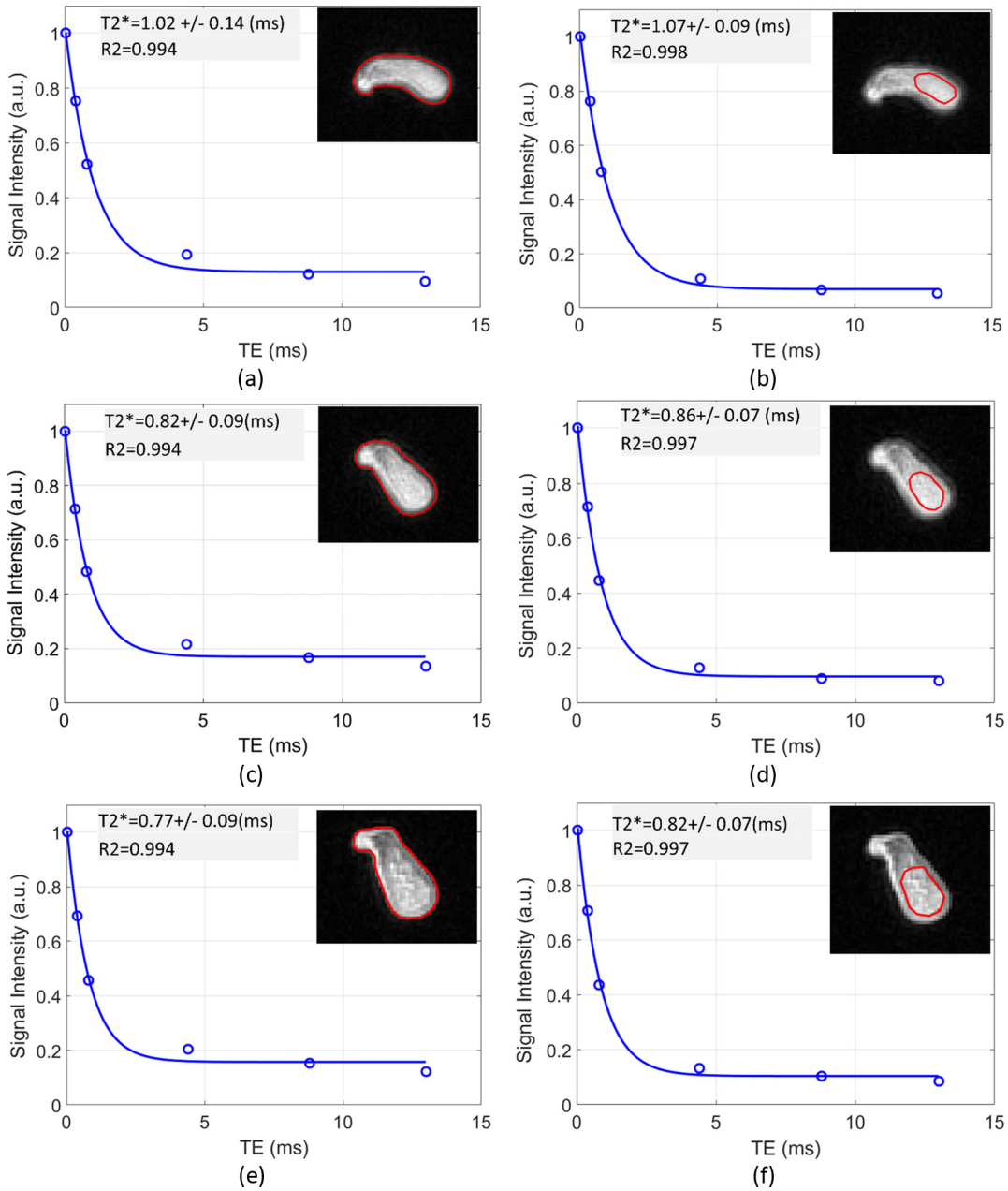

Fig. 2. UTE-MR images with T2* decay curves comparing the three loading conditions in sample B-1. Single component fitting of T2* decay in the whole and the core sections for (a,b) non-loaded (straight), compared with (c,d) 15 and (e,f) 30 N loaded tendons.

Table 1
T2* values from single component decay analyses for all the samples (groups A and B) at different loading steps within the whole and the core sections of tendons.

Sample No	ROI	$T2^*$ (ms)		
		Unloaded	Load 1	Load 2
A-1	Whole	0.47 ± 0.03	0.46 ± 0.03	NA
	Core	0.51 ± 0.04	0.47 ± 0.03	NA
A-2	Whole	1.04 ± 0.08	0.89 ± 0.07	NA
	Core	1.12 ± 0.08	0.90 ± 0.07	NA
A-3	Whole	0.69 ± 0.12	0.68 ± 0.11	NA
	Core	0.59 ± 0.09	0.52 ± 0.06	NA
B-1	Whole	1.02 ± 0.13	0.82 ± 0.09	0.77 ± 0.08
	Core	1.07 ± 0.08	0.86 ± 0.07	0.82 ± 0.07
B-2	Whole	0.47 ± 0.04	0.38 ± 0.03	0.34 ± 0.02
	Core	0.46 ± 0.03	0.37 ± 0.03	0.32 ± 0.03
B-3	Whole	1.23 ± 0.21	1.01 ± 0.19	0.91 ± 0.17
	Core	1.53 ± 0.20	1.22 ± 0.18	1.15 ± 0.17

Table 2
T1 values of all the scanned tendon samples (groups A and B) at different loading steps within the whole and the core sections of tendons.

Sample No	ROI	T1 (ms)		
		Unloaded	Load 1	Load 2
A-1	Whole	610 ± 30	740 ± 40	NA
	Core	640 ± 20	760 ± 40	NA
A-2	Whole	840 ± 20	840 ± 30	NA
	Core	830 ± 30	840 ± 30	NA
A-3	Whole	590 ± 10	630 ± 10	NA
	Core	580 ± 10	590 ± 10	NA
B-1	Whole	900 ± 20	1140 ± 30	810 ± 10
	Core	870 ± 30	1110 ± 40	800 ± 20
B-2	Whole	590 ± 60	570 ± 20	580 ± 20
	Core	590 ± 80	540 ± 20	590 ± 20
B-3	Whole	590 ± 30	620 ± 50	610 ± 10
	Core	660 ± 60	700 ± 70	670 ± 10

however the T2* reduction was less after the second step of loading (30 N).

The estimated T2* of all examined tendons at different loading steps, based on the single component fitting analyses within the whole and the core sections, are presented in Table 1. For all samples in group A and group B, the T2* values were reduced by applying mechanical loads.

Table 2 presents the estimated T1 values, based on the single component fitting analyses within the whole and the core sections of the tendons, at different loading steps. No clear trend for T1 value change was observed, by applying mechanical tensile load. However, for five of the scanned samples, T1 values were increased at the first loading step.

MTR of all the scanned tendon samples (groups A and B) at 2, 5 and 10 kHz off-resonance frequencies for 1500° MT pulse, are presented in Table 3. The MTR change did not show a consistent trend for all scanned tendon samples. However, for most of the cases there was an increase in MTR.

Table 3
Magnetization transfer ratio (MTR) of all the scanned tendon samples (groups A and B) at different loading steps within the whole and the core sections. The MTR is calculated at 2, 5 and 10 kHz off-resonance frequencies for 1500 deg MT power.

Sample No	ROI	MTR (%)								
		Unloaded			Load 1			Load 2		
		2 kHz	5 kHz	10 kHz	2 kHz	5 kHz	10 kHz	2 kHz	5 kHz	10 kHz
A-1	Whole	16.6	12.0	8.6	17.7	12.3	9.0	NA	NA	NA
	Core	15.8	11.5	8.2	17.8	12.3	9.2	NA	NA	NA
A-2	Whole	29.6	22.9	17.6	31.3	23.8	18.2	NA	NA	NA
	Core	30.2	23.2	17.5	31.8	24.2	18.3	NA	NA	NA
A-3	Whole	16.9	11.2	7.3	16.4	12.3	11.0	NA	NA	NA
	Core	22.8	16.1	11.5	22.8	16.6	12.1	NA	NA	NA
B-1	Whole	22.4	17.6	14.0	23.7	17.6	14.4	26.0	18.7	15.6
	Core	24.1	19.3	15.3	24.9	18.1	14.8	26.8	20.0	16.1
B-2	Whole	29.7	20.2	14.9	29.7	19.0	14.6	28.0	18.7	14.2
	Core	32.2	21.2	16.5	32.7	21.0	15.8	32.0	21.9	16.1
B-3	Whole	16.8	12.0	9.4	16.9	12.3	9.5	17.2	12.7	9.4
	Core	20.5	15.5	11.5	20.5	15.0	11.4	20.8	15.0	11.3

Table 4
The summary of changes (%) of T2*, T1 and MTR of all the scanned tendon samples at different loading steps.

	T2* change[a]		T1 change		MTR change					
					2 KHZ		5 KHZ		10 KHZ	
	1st load	2nd load	1st load	2nd load	1st load	2nd load	1st load	2nd load	1st load	2nd load
Whole section	−13 ± 7 (P = 0.028)[b]	−9 ± 2 (P = 0.059)	+10 ± 11 (P = 0.137)	−10 ± 14 (P = 0.428)	+3 ± 4 (P = 0.139)	+2 ± 6 (P = 0.799	+2 ± 5 (P = 0.518)	+3 ± 3 (P = 0.124)	+10 ± 18 (P = 0.215	+2 ± 5 (P = 0.631)
Core section	−16 ± 5 (P = 0.016)	−7 ± 5 (P = 0.121)	+8 ± 12 (P = 0.200)	−8 ± 15 (P = 0.468)	+4 ± 4 (P = 0.052)	+2 ± 4 (P = 0.618)	+1 ± 5 (P = 0.845)	+5 ± 5 (P = 0.045)	2 ± 6 (P = 0.558)	+3 ± 4 (P = 0.388)

[a] All values are presented as Mean ± SD (%). Negative and positive values are representing decrease and increase, respectively.
[b] P-value is calculated from two paired two tailed t student test.

The summary of average changes in T2*, T1 and MTR values within both the ROIs and for both the loading steps are presented in Table 4. The statistical analyses revealed that the mean T2* values for the first step of loading, in the whole and the core sections, were decreased significantly by 13 ± 7% (P = 0.028) and 16 ± 5% (P = 0.017), respectively. For the second loading step, changes in T2* values were not statistically significant, but showed a decreasing trend (9 ± 2% (P = 0.059) and 7 ± 5% (P = 0.121) for whole and core sections, respectively).

Mean T1 value variations were not statistically significant or consistent for the two loading steps, for either of the selected ROIs (Table 4). Although, the mean MTR values were increased slightly by loading within both selected ROIs, the differences were not statistically significant (Table 4). As summarized in Table 4, the T2* was the only studied biomarker that demonstrated significant changes by applying tensile loads consistently for all tendon samples (P < 0.05).

Fig. 3 shows the T2* maps of three different tendon samples as examples (A-2, B-1 and B-2, respectively). The maps are presented at three different loading conditions; non-loaded, 15 and 30 N. The regions of higher T2* (indicated by green to red in the maps) decreased in size by static mechanical loading for all the samples. In other words, the blue regions of lower T2* values were expanding by the loading. Similar local variations in T2* values were observed on the maps of all examined tendon samples in this study.

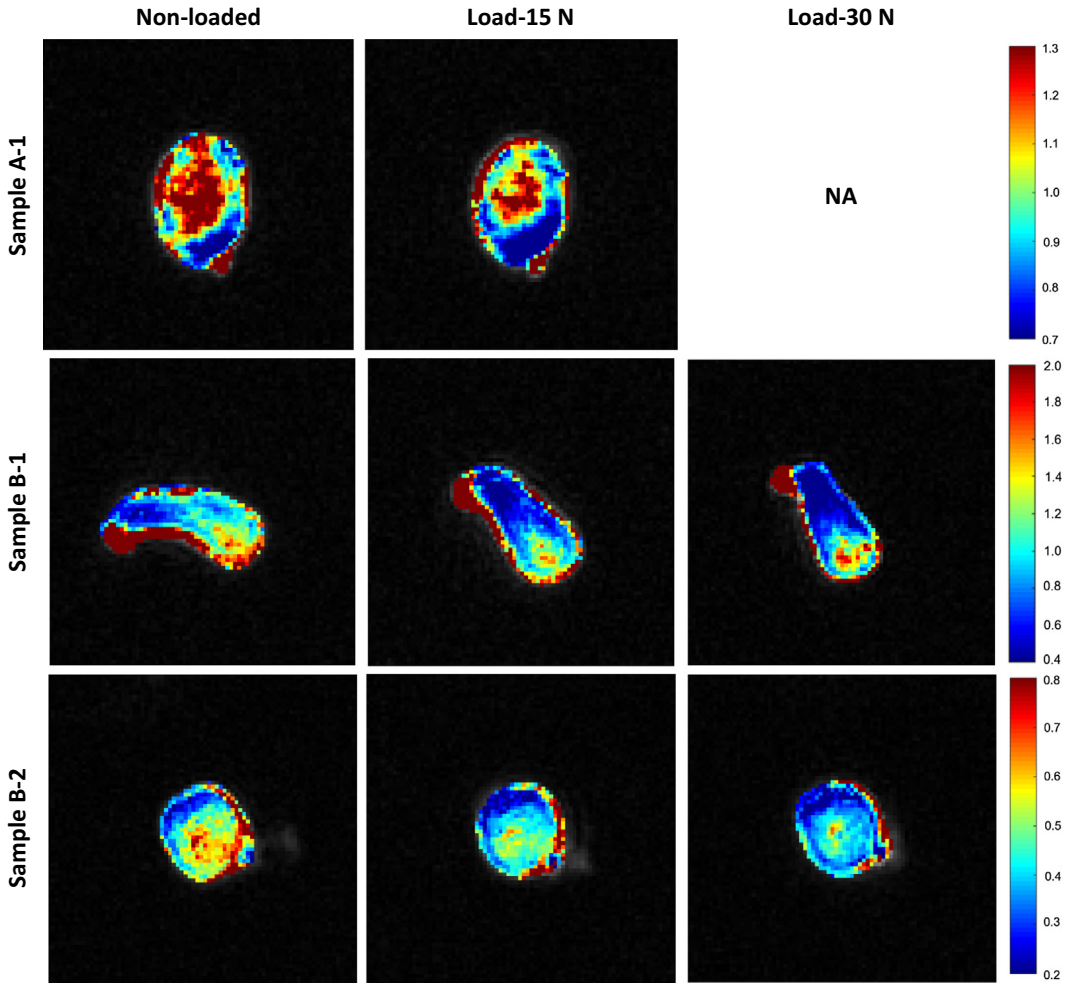

Fig. 3. The T2* map in three selected tendon samples, A-1, B-1 and B-2 at different loading conditions (non-loaded, 15 and 30 N). The regions of higher T2* values (indicated by green to red) of all samples decreased in size within the tendons by mechanical loading.

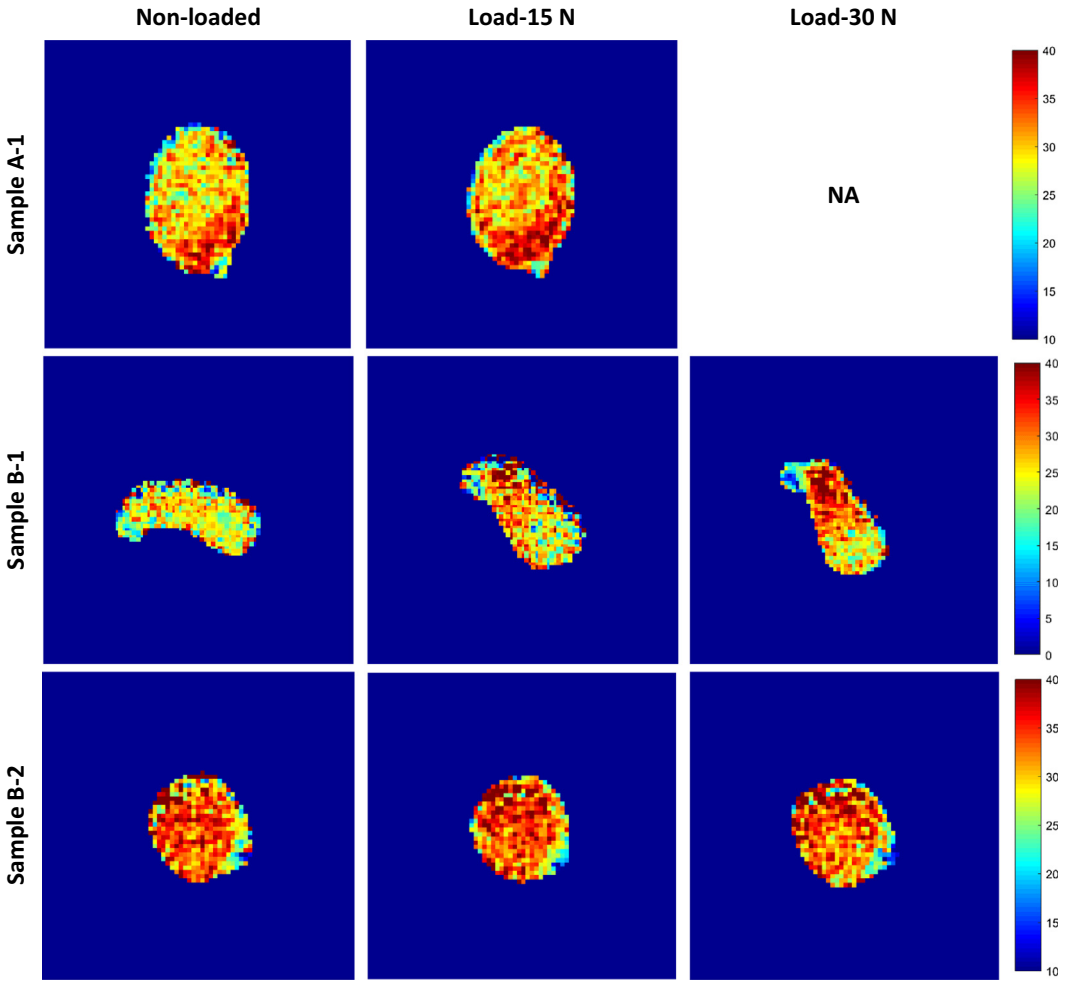

Fig. 4. The magnetization transfer ratio (MTR) maps for different loading conditions (non-loaded, 15 and 30 N) at 2 kHz frequency offset and 1500° MT pulse preparation. The MTR map indicated higher values and non-homogenous distributions for loaded tendons particularly in sample B-1. Sample A-1 and B-2 showed less variations by loading.

Fig. 4 depicts the MTR maps of sample A-1, B-1 and B-2 (same samples in Fig. 3) at different loading conditions. The loading resulted in an inhomogeneous distribution of MTR in sample A-1 with local maxima in the sites of lower T2* values (Fig. 3). The MTR increase was obvious in few samples in this study such as sample B-1, however other example samples (such as sample A-1 and B-2) did not show clear MTR shifts or increase in the maps.

4. Discussion

Human cadaveric peroneal tendons were studied using UTE-MRI under tensile static loading. This study follows prior works using UTE-MRI for assessing loaded tendons (Chang et al., 2015a, 2015c; Koff et al., 2014; Syha et al., 2014). Monitoring the UTE-MRI based biomarkers of tendons under tensile load application may provide an index for the tendon's mechanical performance, which in turn can be used for early stage diagnosis of tendon diseases.

UTE-MTR and T2* were the two studied properties in the literature (Chang et al., 2015a, 2015c; Koff et al., 2014; Syha et al., 2014). UTE-MTR was found to be increasing in vivo after short-term exercises (Syha et al., 2014) and ex vivo under static tensile loads (5–10 N) (Chang et al., 2015a). Koff et al. observed T2* decreasing in tendons after cyclic loading (100 cycles of 45 N) (Koff et al., 2014). Nevertheless, Chang et al. (2015c) did not observe any significant change in T2* of tendons under tensile static loads (10 N). This current study helps to realize the impacts of the load magnitude on the tendon MRI-based properties. It was illustrated that the level of changes in the UTE-MRI properties is a function of the applied load magnitude. Specifically, the level of changes in T2* was higher for 30 N load compared with 15 N load. It is likely that the 10 N load applied in a previous study (Chang et al., 2015c) was not enough to exert any changes in T2*.

The fabricated MRI-compatible loading device with plastic grippers provided a method to apply higher loads compared with our previous study (Chang et al., 2015c). Specifically, by eliminating the need for sutures, we were able to apply > 10 N to the mounted tendons. To the authors' knowledge, the applied loads on the peroneal tendons during daily activities have not been reported in the literature. However, for Achilles tendons, the estimated load peak, during recreational running, may reach up to several times of body weight (Andrew and Jonathan, 2014). This is much higher than applied loads in this study. The loading device employed plastic springs that ended in a very compact and sealed unit which was compatible with a wrist coil, without requiring strings and suspended loads (Chang et al., 2015c; Helmer et al., 2004; Wellen et al., 2005, 2004). However, the plastic spring may have a limited creep and stiffness reduction along the loading process in MRI. To reduce the stiffness changes along the loading experiment, springs underwent four loading sessions from 0 to maximum compression before scanning. Along the four loading sessions, the average calculated stiffness reduced up to 6% and converged to 1.98 N/mm.

Applying the first step static tensile load (15 N) resulted in significant reduction of mean T2* in all scanned tendon samples for

both whole and core sections (13 ± 7% (P = 0.028) and 16 ± 5% (P = 0.017), respectively, Tables 1 and 4). For the second loading step (30 N), the T2* values trended down, but this did not reach statistical significance (Tables 1 and 4). One possible explanation is that the second loading step was performed after an hour of loading by 15 N. Such preconditioning may have prevented the tendons from demonstrating significant changes at the subsequent 30 N load application. T2* reductions were consistent with the observations from Koff et al. (2014) in rabbit patellar tendon after cyclically loaded by 45 N. Therefore, both static and cyclic loadings resulted in similar changes in T2*. The applied load in our previous study (10 N) and the loading set up (suturing strips passing through the syringe and connecting to suspended weights), were likely limited in their ability to exert significant changes in tendons. Likewise, Helmer et al. (2004) did not observe changes in rabbit Achilles when 5 N tensile load was applied.

Of the biomarkers evaluated in our study, T2* was the only one that consistently demonstrated significant changes by applying mechanical loads for all tendon samples. Mean T1 value variations were not statistically significant for both of the loading steps and within both selected ROIs (Table 1 and Table 4). Mean MTR values were increased slightly by loading within both selected ROIs, however, the differences were not statistically significant (Tables 3 and 4).

T2* maps demonstrated a shrinkage of high-T2* regions by the application of tensile load for all scanned tendons (Fig. 3). High-T2* region shrinkage was observed in both core and rim sections of the tendon samples. However, more intense changes were found in the core sections (Fig. 3). Such T2* reductions and shifts were expected due to, first, free water movement from denser regions of tendons towards less dense regions and possibly to both ends of tendon mounted in clamps, and second, reduction of crimp number as well as flattening of crimp angles. Specifically, such crimp reductions and flattening result in an angle decrease between collagen fiber axes and static magnetic field (B0), which in turn leads to lower T2* values. The lowest and highest values of T2* could be found at 0° and 55° angles with respect to B0 (Chang et al., 2015 b; Mengiardi et al., 2006; Mountain et al., 2011). The T2* map shifts were not perfectly homogenous, probably due to uneven mechanical stress distribution in tendon cross sections (Slane and Thelen, 2014). Interestingly, the loading led to a slight increase of MTR in the sites of lower T2* values (Figs. 3 and 4) which agrees with MTR increases, observed by Syha et al. (2014) in vivo and by Chang et al. (2015a) in vitro. Nevertheless, the MTR increase was obvious only in few samples of this study such as sample B-1 (Fig. 4).

Despite the UTE-MRI techniques, the cilinical MRI has been used very often for loaded tendon studies. Helmer et al. (2004) investigated tendon proton density to monitor intra-tendinous water movement after mechanical loading. Proton density demonstrated an increase in the rim sections of tendons while a decrease was seen in the core sections with 10 N loads, indicating outward water shifts (Helmer et al., 2004). Remarkably, for a lower tensile load (5 N), no change was observed in the core section. Wellen et al. (2005) studied T2 and T1 of tendons under loading. T2 increased in the rim but decreased in the core sections of tendon after loading. T1 decreased in both rim and core regions (Wellen et al., 2005). Repeated tensile loads after a period of unloading resulted in similar changes in T2 (Helmer et al., 2006). Mountain et al. (2011) also reported a significant T2 increase in tendons after static tensile loading, however the tendons were fixed in formalin after loading. They also examined the tendons in different orientation angles with respect to B0 direction. The T2 values were higher in loaded tendons for all orientation angles (Mountain et al., 2011). Apparent diffusion coefficient (ADC) was also invesitaed in other studies (Han et al., 2000; Wellen et al., 2004). A significant increase in ADC was observed and interpreted as a sign of water reduction in the tendons (Han et al., 2000), particularly in the tendon core (Wellen et al., 2004).

This study has several limitations. First, a small number of samples were included. As is the nature of pilot studies, our results require a validation with larger sampling sizes. Furthermore, our tendon specimens were obtained from a wide span in age of subjects and future studies should evaluate the possible effects of age. Second, the T2* calculations were performed using single-component exponential models. Future studies will include bi-component models to investigate whether the T2* reduction occurrs in the short or long T2* components of the tissue. It should be noted that the bi-component models require more data points with higher signal-to-noise ratio in order to ensure appropriate fitting. Third, the tendon samples were scanned only parallel to B0 direction. Although the T2* reductions can be explained by changes related to water movement, the reduction and flattening of crimps may also play a role. Future studies evaluating T2* may incorporate other tendon orientations, such as scanning at the magic angle (55°), for a comprehensive understanding of UTE-MRI changes of tendon under loading. Moreover, future studies may consider incorporating biomarkers that are known to be less sensitive to orientation angle, such as those generated from UTE-MT with two-pool modeling (Ma et al., 2016, 2017). Fourth, the employed plastic springs may demonstrate limited creep during the loading process and MRI scanning. Future studies should employ active MRI-compatible actuators (e.g., pneumatic actuators) to achieve higher accuracy and reliability. Finally, the degree of change in loaded healthy versus pathologic tendons would be of interest in future studies.

5. Conclusion

This study investigates the mechanical status of tendons through observations in UTE-MRI biomarkers. T2*, T1, and MTR values were measured for human peroneal tendons before and under static tensile mechanical loads. Among examined MRI properties, only T2* demonstrated significant changes under mechanical loading (over 12% reduction). T2* maps revealed a significant shrinkage of high-T2* regions in tendon cross sections which might be caused by, first, intra-tendinous shifts in water and second, alterations in tendon crimp. T2* monitoring over the course of loading can be suggested as a new technique for quantitative investigation of the tendons biomechanics.

Acknowledgements

The authors thank Niloofar Shojaeiadib for performing the statistical analyses. The authors acknowledge grant support from the VA (I01CX001388) and NIH (1R01 AR062581-01A1 and 1 R01 AR068987-01).

Conflict of interest statement

The authors have no conflict of interests to disclose.

References

Aparecida de Aro, A., de Campos Vidal, B., Pimentel, E.R., 2012. Biochemical and anisotropical properties of tendons. Micron 43, 205–214. http://dx.doi.org/10.1016/j.micron.2011.07.015.

Chang, E.Y., Bae, W.C., Statum, S., Du, J., Chung, C.B., 2014a. Effects of repetitive freeze-thawing cycles on T2 and T2* of the Achilles tendon. Eur. J. Radiol. 83, 349–353. http://dx.doi.org/10.1016/j.ejrad.2013.10.014.

Chang, E.Y., Du, J., Bae, W.C., Statum, S., Chung, C.B., 2014b. Effects of Achilles tendon immersion in saline and perfluorochemicals on T2 and T2*. J. Magn. Reson. Imaging 40, 496–500. http://dx.doi.org/10.1002/jmri.24360.

Chang, E.Y., Du, J., Biswas, R., Statum, S., Pauli, C., Bae, W.C., Chung, C.B., 2015a. Off-resonance saturation ratio obtained with ultrashort echo time-magnetization transfer techniques is sensitive to changes in static tensile loading of tendons and degeneration. J. Magn. Reson. Imaging 42, 1064–1071. http://dx.doi.org/10.1002/jmri.24881.

Chang, E.Y., Du, J., Chung, C.B., 2015b. UTE imaging in the musculoskeletal system. J. Magn. Reson. Imaging 41, 870–883. http://dx.doi.org/10.1002/jmri.24713.

Chang, E.Y., Du, J., Iwasaki, K., Biswas, R., Statum, S., He, Q., Bae, W.C., Chung, C.B., 2015c. Single- and Bi-component T2Star analysis of tendon before and during tensile loading, using UTE sequences. J. Magn. Reson. Imaging 42, 114–120. http://dx.doi.org/10.1002/jmri.24758.

Du, J., Carl, M., Bydder, M., Takahashi, A., Chung, C.B., Bydder, G.M., 2010a. Qualitative and quantitative ultrashort echo time (UTE) imaging of cortical bone. J. Magn. Reson. 207, 304–311. http://dx.doi.org/10.1016/j.jmr.2010.09.013.

Du, J., Chiang, A.J.T., Chung, C.B., Statum, S., Znamirowski, R., Takahashi, A., Bydder, G.M., 2010b. Orientational analysis of the Achilles tendon and enthesis using an ultrashort echo time spectroscopic imaging sequence. Magn. Reson. Imaging 28, 178–184. http://dx.doi.org/10.1016/j.mri.2009.06.002.

Franchi, M., Fini, M., Quaranta, M., De Pasquale, V., Raspanti, M., Giavaresi, G., Ottani, V., Ruggeri, A., 2007a. Crimp morphology in relaxed and stretched rat Achilles tendon. J. Anat. 210, 1–7. http://dx.doi.org/10.1111/j.1469-7580.2006.00666.x.

Franchi, M., Trirè, A., Quaranta, M., Orsini, E., Ottani, V., 2007b. Collagen structure of tendon relates to function. ScientificWorldJournal. 7, 404–420. http://dx.doi.org/10.1100/tsw.2007.92.

Han, S., Gemmell, S.J., Helmer, K.G., Grigg, P., Wellen, J.W., Hoffman, a.H., Sotak, C.H., 2000. Changes in ADC caused by tensile loading of rabbit achilles tendon: evidence for water transport. J. Magn. Reson. 144, 217–227. http://dx.doi.org/10.1006/jmre.2000.2075.

Hannafin, J.A., Arnoczky, S.P., 1994. Effect of cyclic and static tensile loading on the water content and solute diffusion in canine flexor tendons: An in vitro study. J. Orthop. Res. 12, 350–356.

Hansen, K.A., Weiss, J.A., Barton, J.K., 2002. Recruitment of tendon crimp with applied tensile strain. J. Biomech. Eng. 124, 72–77. http://dx.doi.org/10.1115/1.1427698.

Helmer, K.G., Nair, G., Cannella, M., Grigg, P., 2006. Water movement in tendon in response to a repeated static tensile load using one-dimensional magnetic resonance imaging. J. Biomech. Eng. 128, 733–741. http://dx.doi.org/10.1115/1.2244573.

Helmer, K.G., Wellen, J., Grigg, P., Sotak, C.H., 2004. Measurement of the Spatial Redistribution of Water in Rabbit Achilles Tendon in Response to Static Tensile Loading. J. Biomech. Eng. 126, 651. http://dx.doi.org/10.1115/1.1800573.

Hendee, W.R., Morgan, C.J., 1984. Magnetic resonance imaging. Part I–physical principles. West. J. Med. 141, 491–500.

Jerban, S., Nazaran, A., Carl, M., Cheng, X., Chang, E.Y., Du, J., 2017. The effect of loading on T2* and MT ratio in tendons: A feasibility study. In: Proc. Intl. Soc. Mag. Reson. Med. 25 (2017). p. Poster 1535.

Juras, V., Apprich, S., Szomolanyi, P., Bieri, O., Deligianni, X., Trattnig, S., 2013. Bi-exponential T2*analysis of healthy and diseased Achilles tendons: An in vivo preliminary magnetic resonance study and correlation with clinical score. Eur. Radiol. 23, 2814–2822. http://dx.doi.org/10.1007/s00330-013-2897-8.

Juras, V., Zbyn, S., Pressl, C., Valkovic, L., Szomolanyi, P., Frollo, I., Trattnig, S., 2012. Regional variations of T2* in healthy and pathologic achilles tendon in vivo at 7 Tesla: preliminary results. Magn. Reson. Med. 68, 1607–1613. http://dx.doi.org/10.1002/mrm.24136.

Khan, K.M., Cook, J.L., Bonar, F., Harcourt, P., Astrom, M., 1999. Histopathology of common tendinopathies: update and implications for clinical management. Sport. Med. 27, 393–408. http://dx.doi.org/10.2165/00007256-199927060-00004.

Koff, M.F., Powndler, S.L., Shah, P.H., Yang, L.W., Potter, H.G., 2014. Ultrashort echo imaging of cyclically loaded rabbit patellar tendon. J. Biomech. 47, 3428–3432. http://dx.doi.org/10.1016/j.jbiomech.2014.08.018.

Legerlotz, K., Dorn, J., Richter, J., Rausch, M., Leupin, O., 2014. Age-dependent regulation of tendon crimp structure, cell length and gap width with strain. Acta Biomater. 10, 4447–4455. http://dx.doi.org/10.1016/j.actbio.2014.05.029.

Ma, Y.-J., Chang, E.Y., Carl, M., Du, J., 2017. Quantitative magnetization transfer ultrashort echo time imaging using a time-efficient 3D multispoke Cones sequence. Magn. Reson. Med., 1–9 http://dx.doi.org/10.1002/mrm.26716.

Ma, Y.-J., Shao, H., Du, J., Chang, E.Y., 2016. Ultrashort echo time magnetization transfer (UTE-MT) imaging and modeling: magic angle independent biomarkers of tissue properties. NMR Biomed. 29, 1546–1552. http://dx.doi.org/10.1002/nbm.3609.

Mengiardi, B., Pfirrmann, C.W.A., Schöttle, P.B., Bode, B., Hodler, J., Vienne, P., Zanetti, M., 2006. Magic angle effect in MR imaging of ankle tendons: Influence of foot positioning on prevalence and site in asymptomatic subjects and cadaveric tendons. Eur. Radiol. 16, 2197–2206. http://dx.doi.org/10.1007/s00330-006-0164-y.

Morgan, M., Kostyuk, O., Brown, R.A., Mudera, V., 2006. In situ monitoring of tendon structural changes by elastic scattering spectroscopy: correlation with changes in collagen fibril diameter and crimp. Tissue Eng. 12, 1821–1831. http://dx.doi.org/10.1089/ten.2006.12.ft-84.

Mountain, K.M., Bjarnason, T.A., Dunn, J.F., Matyas, J.R., 2011. The functional microstructure of tendon collagen revealed by high-field MRI. Magn. Reson. Med. 66, 520–527. http://dx.doi.org/10.1002/mrm.23036.

Nazaran, A., 2016. Ultra Short MR Relaxometry and Histological Image Processing for Validation of Diffusion MRI. Brigham Young University.

Nazaran, A., Tarbox, G., Hartley, R., Bangerter, N., 2017. Difference image ultra-short echo time T2* mapping using a 3D cones trajectory. In: Proc. Intl. Soc. Mag. Reson. Med. 25 (2017). p. Poster 0374.

Pierre-Jerome, C., Moncayo, V., Terk, M.R., 2010. MRI of the Achilles tendon: a comprehensive review of the anatomy, biomechanics, and imaging of overuse tendinopathies. Acta radiol. 51, 438–454. http://dx.doi.org/10.3109/02841851003627809.

Shao, H., Chang, E.Y., Pauli, C., Zanganeh, S., Bae, W., Chung, C.B., Tang, G., Du, J., 2016. UTE bi-component analysis of T2* relaxation in articular cartilage. Osteoarthr. Cartil. 24, 364–373. http://dx.doi.org/10.1016/j.joca.2015.08.017.

Slane, L.C., Thelen, D.G., 2014. Non-uniform displacements within the Achilles tendon observed during passive and eccentric loading. J. Biomech. 47, 2831–2835. http://dx.doi.org/10.1016/j.jbiomech.2014.07.032.

Syha, R., Springer, F., Grözinger, G., Würslin, C., Ipach, I., Ketelsen, D., Schabel, C., Gebhard, H., Hein, T., Martirosian, P., Schick, F., Claussen, C.D., Grosse, U., 2014. Short-term exercise-induced changes in hydration state of healthy achilles tendons can be visualized by effects of off-resonant radiofrequency saturation in a three-dimensional ultrashort echo time MRI sequence applied at 3 Tesla. J. Magn. Reson. Imaging 40, 1400–1407. http://dx.doi.org/10.1002/jmri.24488.

Wellen, J., Helmer, K.G., Grigg, P., Sotak, C.H., 2005. Spatial characterization of T1 and T2 relaxation times and the water apparent diffusion coefficient in rabbit Achilles tendon subjected to tensile loading. Magn. Reson. Med. 53, 535–544. http://dx.doi.org/10.1002/mrm.20361.

Wellen, J., Helmer, K.G., Grigg, P., Sotak, C.H., 2004. Application of porous-media theory to the investigation of water ADC changes in rabbit Achilles tendon caused by tensile loading. J. Magn. Reson. 170, 49–55. http://dx.doi.org/10.1016/j.jmr.2004.04.021.